Electronic Supplementary Information

Probing a microviscosity change at the nematic-isotropic liquid crystal phase transition by a ratiometric flapping fluorophore

Ryo Kimura,[a] Hidetsugu Kitakado,[a] Takuya Yamakado,[a] Hiroyuki Yoshida,*[b] and Shohei Saito*[a]

[a] Graduate School of Science, Kyoto University, Kitashirakawa Oiwake, Sakyo, Kyoto 606-8502, Japan

[b] Graduate School of Engineering, Osaka University, 2-1 Yamadaoka, Suita, Osaka 565-0871, Japan

Corresponding Authors

yoshida@eei.eng.osaka-u.ac.jp

saito.shohei.4c@kyoto-u.ac.jp

Contents

1. General information

Synthesis

All reagents and solvents were of commercial grade and were used without further purification unless otherwise noted. Benzonitrile (PhCN) was distilled before optical measurements. **FLAP0**[S1], **FLAP1**[S2], **Wing1**[S2], and BODIPY-C$_{12}$[S3] were synthesized according to the reported methods.

Measurements

All optical measurements were performed under air-saturated condition. In Chapter 2, excitation light and emissions were non-polarized. UV-visible absorption spectra were recorded on a Shimadzu UV-3600 spectrometer. Steady-state fluorescence and excitation spectra were recorded on a JASCO FP-8500 spectrofluorometer. Absolute fluorescence quantum yields were determined by an integrating sphere system on a HAMAMATSU C9920-02S apparatus. Fluorescence lifetimes were measured on a compact fluorescence lifetime spectrometer Hamamatsu Photonics QuantaurusTau C11367. Optical measurements were conducted using a 1-cm square quartz cell in PhCN, and 1-mm quartz cell in 5CB. Measurements of temperature-dependent FL spectra and FL lifetimes were conducted on a UNISOKU CoolSpeK UV USP-203-B cryostat connected with a JASCO FP-8500 or a Hamamatsu Photonics QuantaurusTau C11367. Shear viscosity of 5CB was measured on an Anton Paar MCR702 rheometer. Differential scanning calorimetry (DSC) was recorded on a Hitachi High-Tech TA7000.

In Chapter 3, the optical set-up and measurement conditions were shown in the following Figures.
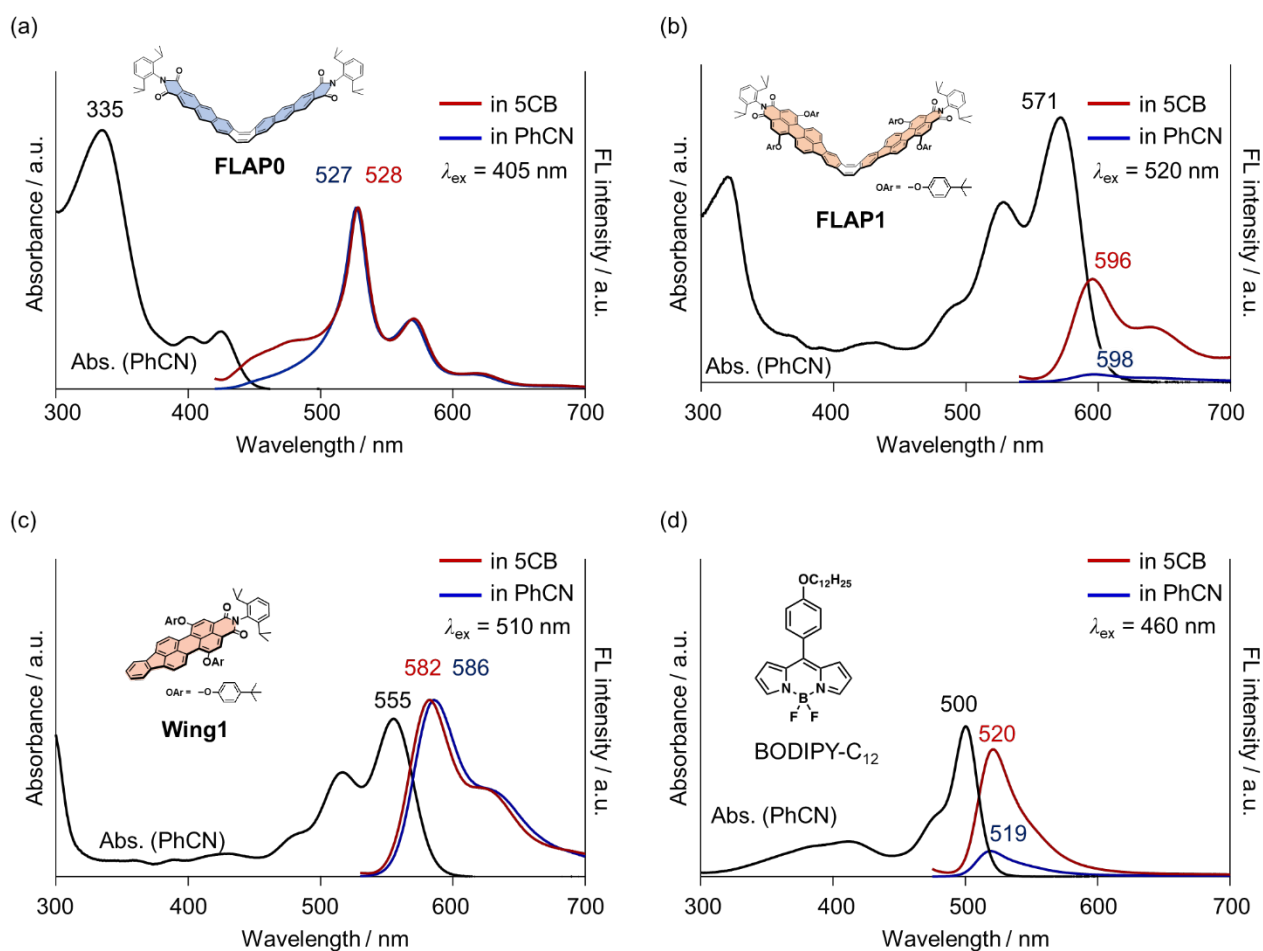
2. Photophysical, rheological, and thermal analyses

Fig. S2-1. UV-visible absorption and FL spectra of (a) **FLAP0**, (b) **FLAP1**, (c) **Wing1**, and (d) BODIPY-C_{12} in PhCN and 5CB. Excitation wavelengths: 405 nm for **FLAP0**, 520 nm for **FLAP1**, 510 nm for **Wing1**, and 460 nm for BODIPY-C_{12}. The FL intensities in (a) and (c) are normalized, while the FL intensities in (b) and (d) are presented to account for the relative FL quantum yields.
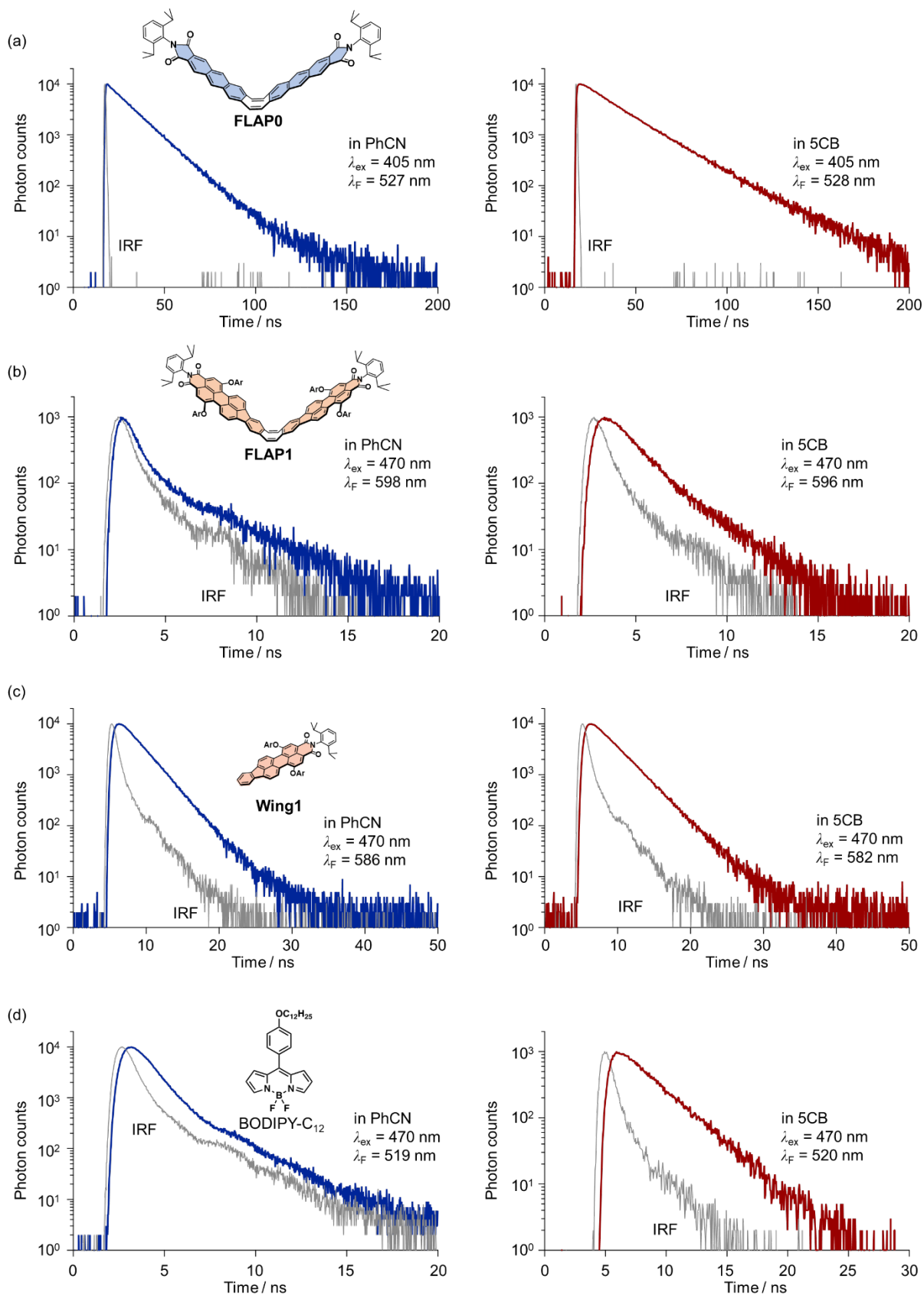
Fig. S2-2. FL decay profiles of (a) **FLAP0**, (b) **FLAP1**, (c) **Wing1**, and (d) BODIPY-C_{12} in PhCN (left) and 5CB (right). Excitation and fluorescence wavelengths are shown in each panel.

Table S2-1. FL quantum yield Φ_F and FL lifetime τ_F of **FLAP0**, **FLAP1**, **Wing1**, and BODIPY-C$_{12}$ in PhCN and 5CB.

Compounds	Solvents	Φ_F[a]	τ_{F1}	τ_{F2}	A_1	A_2	χ^2
FLAP0	PhCN	0.44	0.13 ns[b]	13 ns	−1840 [b]	2270	1.22
	5CB	0.48	0.62 ns [b]	20 ns	−1290 [b]	2440	1.68
FLAP1	PhCN	0.008	0.11 ns [b]	2.8 ns	170 [b]	1.5	1.14
	5CB	0.11	1.1 ns				1.22
Wing1	PhCN	0.37	2.2 ns				1.18
	5CB	0.46	2.6 ns				1.30
BODIPY-C$_{12}$	PhCN	0.056	0.62 ns				1.42
	5CB	0.26	2.2 ns				1.29

[a] Excitation wavelengths for the determination of Φ_F: λ_{ex} = 405 nm (**FLAP0**), λ_{ex} = 520 nm (**FLAP1**), λ_{ex} = 510 nm (**Wing1**), and λ_{ex} = 460 nm (BODIPY-C$_{12}$).

[b] FL lifetime was fitted with $f(t) = A_1 \exp(-t/\tau_{F1}) + A_2 \exp(-t/\tau_{F2})$. Short-lived components ($\tau_1 < 1$ ns) of **FLAP0** obtained as negative A_1 values would originate from planarization dynamics in the excited state.[S2]

Note: The value of the lifetime less than 0.2 ns would include a large margin of error due to being close to the detection limit.
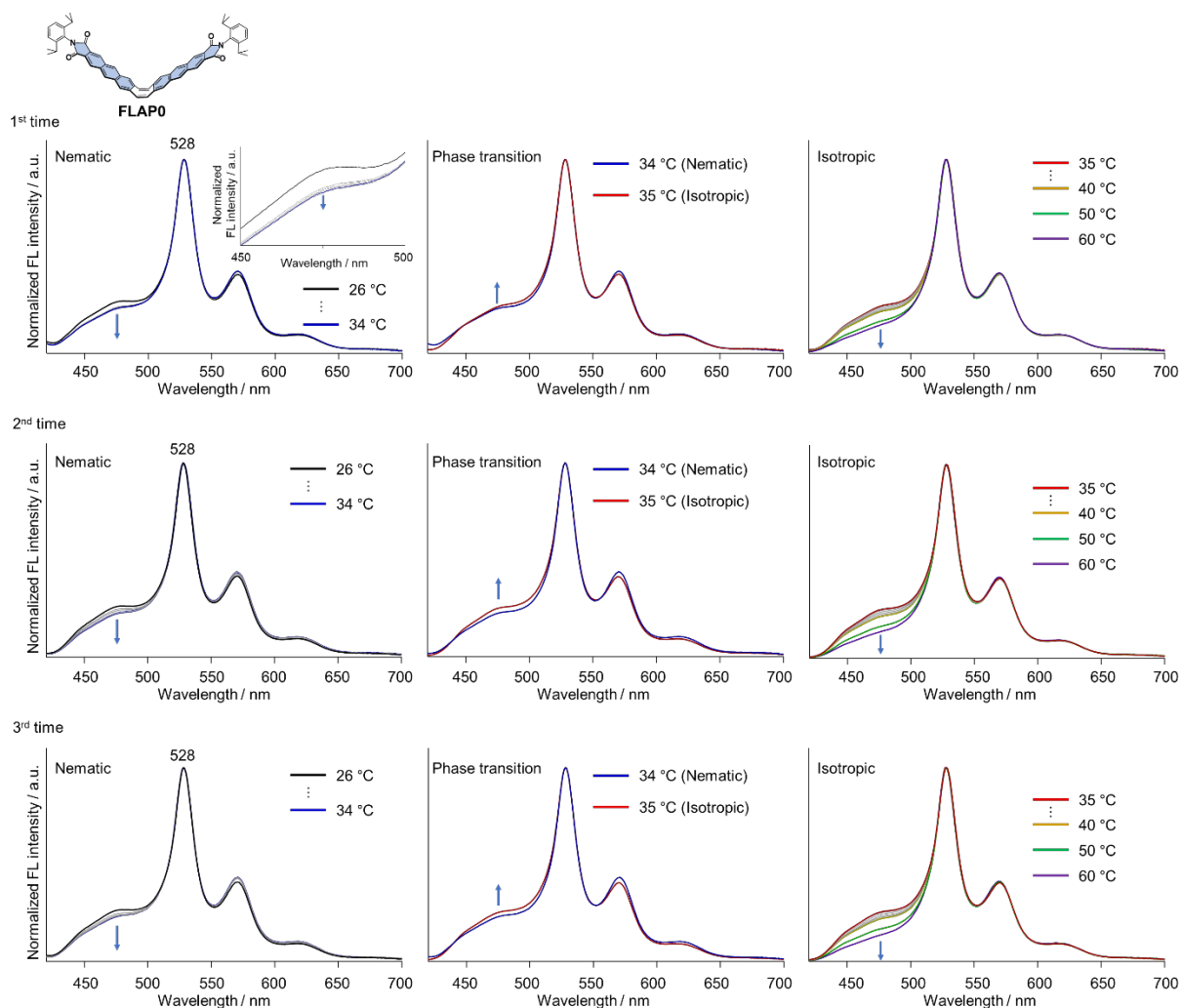
Fig. S2-3. Temperature-dependent FL spectra of **FLAP0** in 5CB (λ_{ex} = 405 nm). The measurements were performed three times. Heating rate: *ca.* 1 °C min^{-1}. Each spectrum was normalized at 528 nm.

Table S2-2. Temperature-dependent FL ratio of **FLAP0** in 5CB (λ_{ex} = 405 nm) for the three measurements.

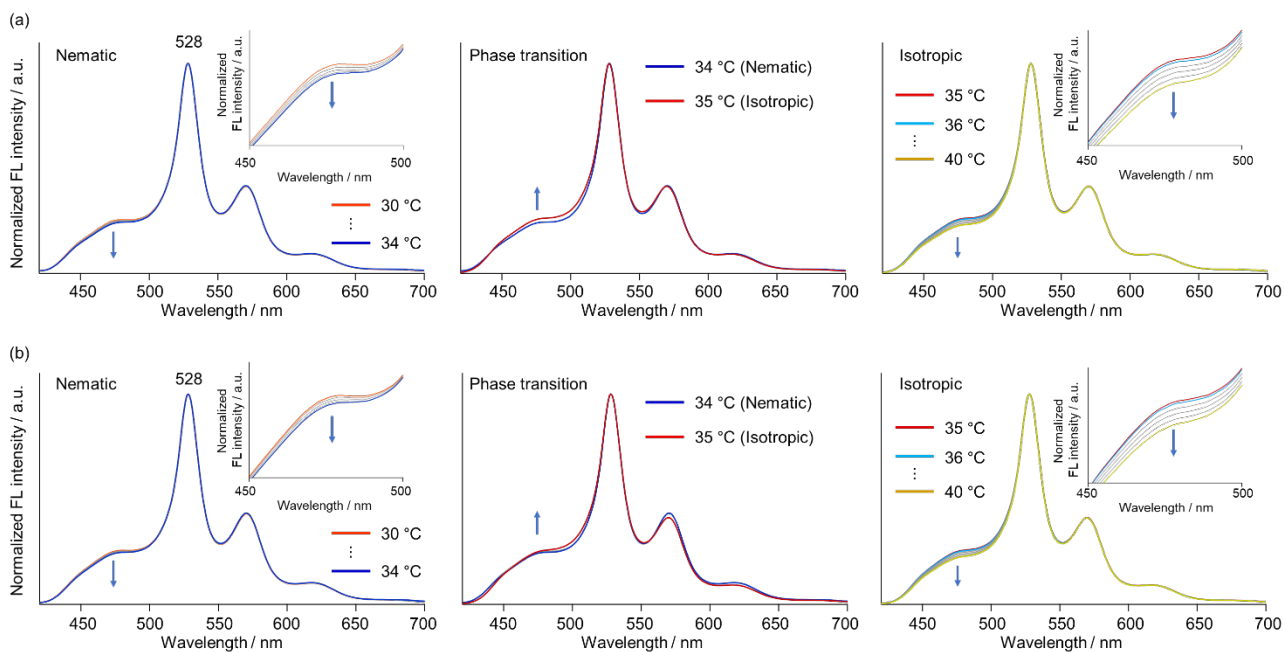| Temperature / °C		FL ratio (I_{528} / I_{475})		
		1st	2nd	3rd
Nematic	26	3.78	3.86	3.81
	30	4.22	4.11	4.10
	31	4.26	4.22	4.23
	32	4.29	4.45	4.28
	33	4.36	4.44	4.30
	34	4.34	4.47	4.34
Isotropic	35	4.16	4.01	3.96
	36	4.25	4.11	4.03
	37	4.35	4.23	4.18
	38	4.50	4.36	4.34
	39	4.62	4.53	4.47
	40	4.71	4.68	4.61
	50	6.14	6.15	6.03
	60	7.00	7.37	7.45

Fig. S2-4. Temperature-dependent FL spectra of **FLAP0** in 5CB (λ_{ex} = 405 nm) in the heating rate of (a) *ca.* 0.5 °C min^{-1} and (b) *ca.* 0.1 °C min^{-1} by manual control. Each spectrum was normalized at 528 nm.

Table S2-3. Temperature-dependent FL ratio of **FLAP0** in 5CB (λ_{ex} = 405 nm) at various heating rate.

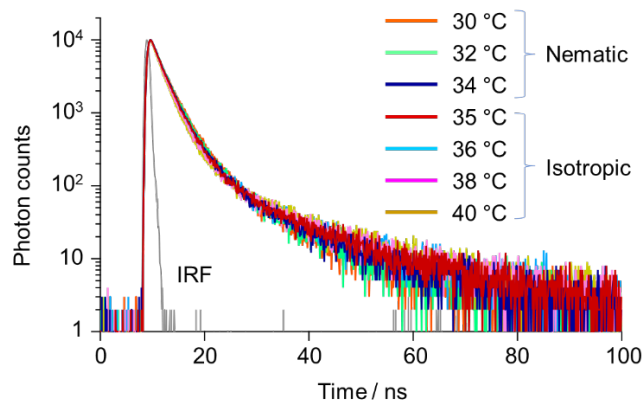| Temperature / °C		FL ratio (I_{528} / I_{475})	
		0.5 °C / min	0.1 °C / min
Nematic	30	3.97	3.96
	31	4.04	4.00
	32	4.09	4.05
	33	4.15	4.10
	34	4.18	4.12
Isotropic	35	3.90	4.00
	36	3.94	4.04
	37	4.05	4.15
	38	4.17	4.27
	39	4.29	4.40
	40	4.42	4.53

Fig. S2-5. Temperature-dependent FL decay profiles of **FLAP0** in 5CB (λ_{ex} = 405 nm and λ_F = 475 nm).

Table S2-4. Temperature-dependent FL lifetime of **FLAP0** in 5CB (λ_{ex} = 405 nm, and λ_F = 475 nm) with (a) double exponential fitting and (b) triple exponential fitting.

(a) Double exponential fitting

	Temperature / °C	τ_{F1}	τ_{F2}	A_1	A_2	χ^2
Nematic	30	2.3 ns	6.8 ns	1270	130	1.64
	32	2.3 ns	7.2 ns	1330	110	1.68
	34	2.3 ns	8.3 ns	1380	77	1.49
Isotropic	35	2.3 ns	9.4 ns	1380	61	1.77
	36	2.3 ns	10 ns	1370	52	1.77
	38	2.2 ns	10 ns	1390	51	1.89
	40	2.1 ns	11 ns	1410	44	1.69

FL lifetime was fitted with $f(t) = A_1 \exp(-t/\tau_{F1}) + A_2 \exp(-t/\tau_{F2})$.

(b) Triple exponential fitting

	Temperature / °C	τ_{F1}	τ_{F2}	τ_{F3}	A_1	A_2	A_3	χ^2
Nematic	30	1.8 ns	3.6 ns	15 ns	810	610	18	1.09
	32	1.6 ns	3.2 ns	12 ns	690	770	29	1.16
	34	1.9 ns	3.6 ns	15 ns	1020	440	19	1.08
Isotropic	35	1.6 ns	3.1 ns	16 ns	730	750	23	1.14
	36	2.0 ns	3.8 ns	18 ns	1140	310	17	1.27
	38	1.9 ns	3.8 ns	19 ns	1180	290	16	1.35
	40	1.7 ns	3.1 ns	17 ns	1030	450	23	1.15

FL lifetime was fitted with $f(t) = A_1 \exp(-t/\tau_{F1}) + A_2 \exp(-t/\tau_{F2}) + A_3 \exp(-t/\tau_{F3})$.

Note: The τ_{F2} component in the double exponential fitting may reflect the microviscosity change during the phase transition, but the reliability is not higher than the ratiometric fluorescence analysis. The triple exponential fitting improved the χ^2 values, but it became more difficult to rationally assign and interpret those components
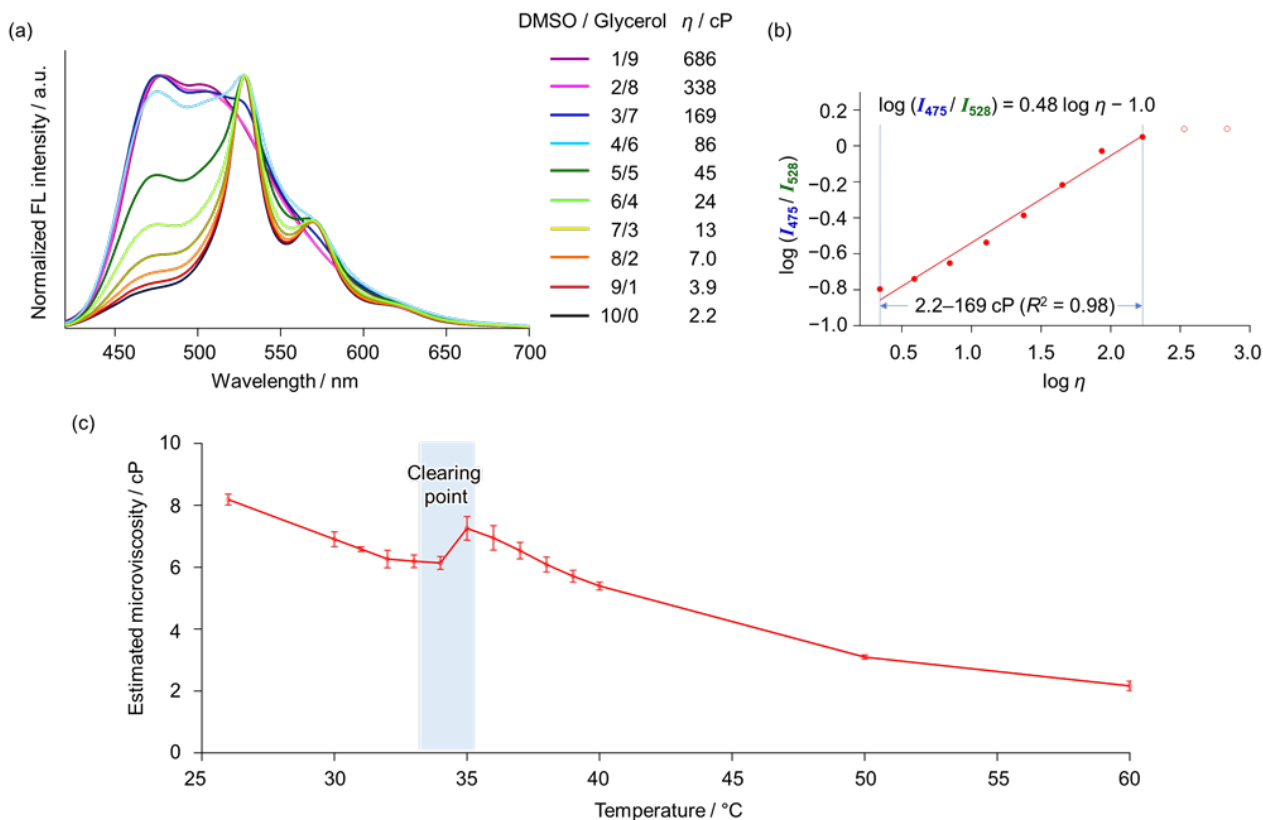
Fig. S2-6. (a) Viscosity-dependent FL spectra of **FLAP0** in mixed solvents of DMSO/glycerol (*v/v*). Excitation by non-polarized light (λ_{ex} = 405 nm). (b) The corresponding Förster–Hoffman plot between 2.2 cP to 169 cP. (c) Microviscosity of 5CB at each temperature estimated from the Förster–Hoffman calibration of **FLAP0**. Measurements were performed 3 times to display sample standard deviation. The microviscosity of 5CB was formally estimated as 6.1 ± 0.2 cP at 34 °C and 7.3 ± 0.4 cP at 35 °C, although the anisotropy of the FL ratio (See Chapter 3) was not considered in these values.

Note: The previously reported Förster–Hoffman plot[S4] was corrected as a double logarithmic graph from the same dual fluorescence spectra.

Table S2-5. Estimated microviscosity of 5CB and PhCN from three FL viscosity probes at about 25 °C.

Viscosity probes	Estimated viscosity of PhCN	Estimated viscosity of 5CB
FLAP0	1.3 cP	8.2 cP
FLAP1	0.3 cP	–
BODIPY-C_{12}	–	340 cP
Rheometer (Shear viscosity at 25 °C)	1.2 cP	21 cP

Note: Each calibration line (FL ratio *vs.* viscosity or FL lifetime *vs.* viscosity) was obtained for **FLAP0** (Fig. S2-6(b)), **FLAP1**[S5] and BODIPY-C_{12}[S6]. By using the calibrations (Förster–Hoffman equations), the viscosities of PhCN and 5CB were estimated. Here, it should be noted that the shear viscosity of 5CB (21 cP) was outside the upper limit of the viscosity range validated by the **FLAP1** calibration (0.3–3.1 cP[S5]). Similarly, the shear viscosity of PhCN (1.2 cP) was outside the lower limit of the calibrated range of BODIPY-C_{12} (15–1500 cP[S6]). In addition, the FL lifetime of **FLAP1** is considerably dependent not only on the microviscosity but also on the relative permittivity of the surrounding media.[S2]
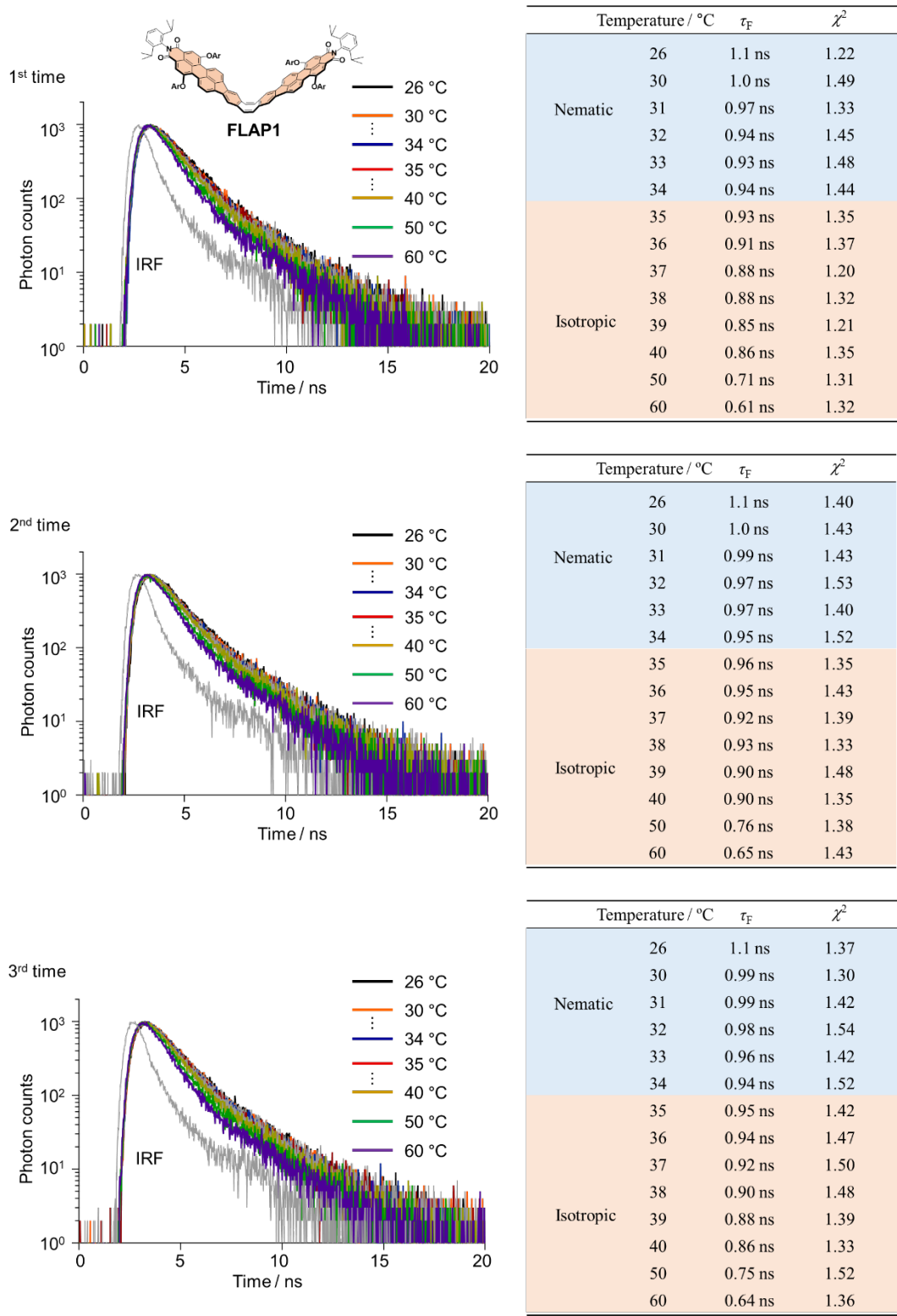
	Temperature / °C	τ_F	χ^2
Nematic	26	1.1 ns	1.22
	30	1.0 ns	1.49
	31	0.97 ns	1.33
	32	0.94 ns	1.45
	33	0.93 ns	1.48
	34	0.94 ns	1.44
Isotropic	35	0.93 ns	1.35
	36	0.91 ns	1.37
	37	0.88 ns	1.20
	38	0.88 ns	1.32
	39	0.85 ns	1.21
	40	0.86 ns	1.35
	50	0.71 ns	1.31
	60	0.61 ns	1.32

	Temperature / °C	τ_F	χ^2
Nematic	26	1.1 ns	1.40
	30	1.0 ns	1.43
	31	0.99 ns	1.43
	32	0.97 ns	1.53
	33	0.97 ns	1.40
	34	0.95 ns	1.52
Isotropic	35	0.96 ns	1.35
	36	0.95 ns	1.43
	37	0.92 ns	1.39
	38	0.93 ns	1.33
	39	0.90 ns	1.48
	40	0.90 ns	1.35
	50	0.76 ns	1.38
	60	0.65 ns	1.43

	Temperature / °C	τ_F	χ^2
Nematic	26	1.1 ns	1.37
	30	0.99 ns	1.30
	31	0.99 ns	1.42
	32	0.98 ns	1.54
	33	0.96 ns	1.42
	34	0.94 ns	1.52
Isotropic	35	0.95 ns	1.42
	36	0.94 ns	1.47
	37	0.92 ns	1.50
	38	0.90 ns	1.48
	39	0.88 ns	1.39
	40	0.86 ns	1.33
	50	0.75 ns	1.52
	60	0.64 ns	1.36

Fig. S2-7. Temperature-dependent FL decay profiles and FL lifetimes of **FLAP1** in 5CB (λ_{ex} = 470 nm and λ_F = 596 nm) for three measurements. The IRF (instrument response function) is displayed in gray.
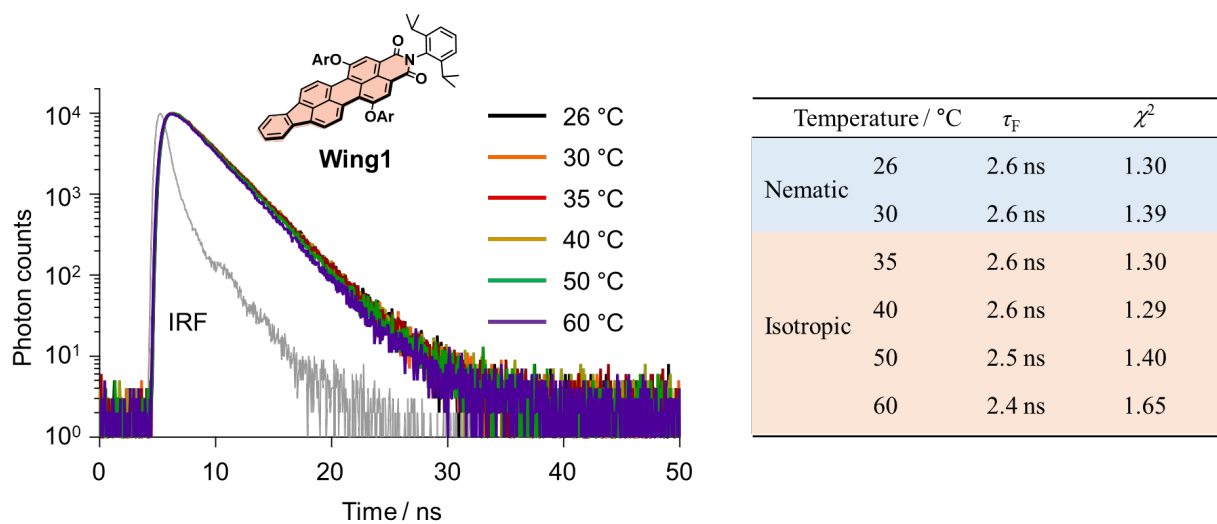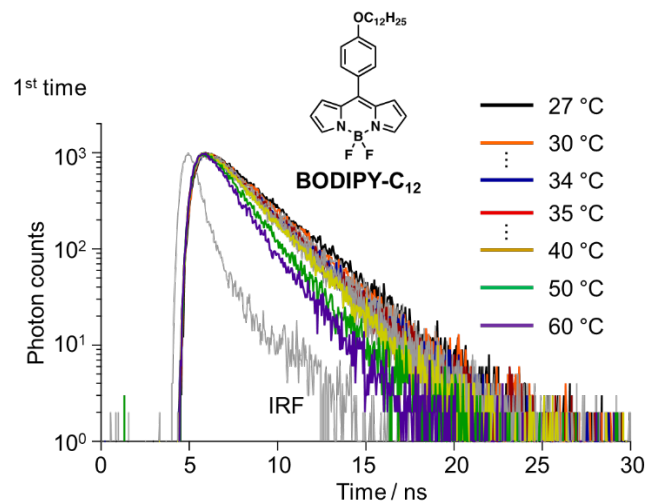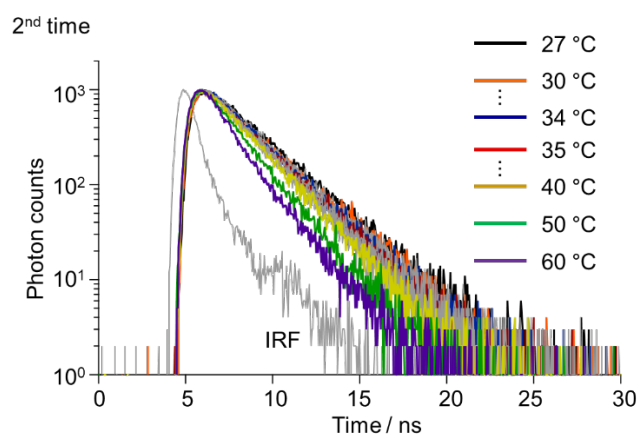
Fig. S2-8. No temperature dependence of FL decay profiles and FL lifetimes of **Wing1** in 5CB (λ_{ex} = 470 nm and λ_F = 582 nm).

1st time

Phase	Temperature / °C	τ_F	χ^2
Nematic	27	2.3 ns	1.11
	30	2.1 ns	1.00
	31	2.0 ns	1.15
	32	2.0 ns	1.28
	33	2.0 ns	1.26
	34	1.9 ns	1.33
Isotropic	35	1.9 ns	1.63
	36	1.9 ns	1.52
	37	1.8 ns	1.49
	38	1.8 ns	1.35
	39	1.8 ns	1.37
	40	1.8 ns	1.35
	50	1.4 ns	1.27
	60	1.1 ns	1.29

2nd time

Phase	Temperature / °C	τ_F	χ^2
Nematic	27	2.2 ns	1.10
	30	2.1 ns	1.46
	31	2.0 ns	1.10
	32	2.0 ns	1.39
	33	1.9 ns	1.24
	34	2.0 ns	1.16
Isotropic	35	1.9 ns	1.30
	36	1.9 ns	1.29
	37	1.8 ns	1.23
	38	1.8 ns	1.01
	39	1.7 ns	1.30
	40	1.8 ns	1.44
	50	1.4 ns	1.19
	60	1.1 ns	1.07

3rd time
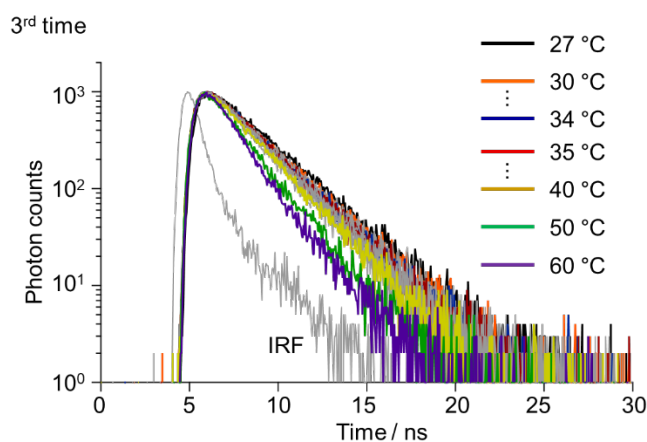
Phase	Temperature / °C	τ_F	χ^2
Nematic	27	2.2 ns	1.22
	30	2.1 ns	1.34
	31	2.0 ns	1.40
	32	2.0 ns	1.16
	33	2.0 ns	1.30
	34	1.9 ns	1.39
Isotropic	35	1.9 ns	1.19
	36	1.9 ns	1.29
	37	1.8 ns	1.17
	38	1.8 ns	1.35
	39	1.7 ns	1.34
	40	1.7 ns	1.43
	50	1.4 ns	1.34
	60	1.1 ns	1.07

Fig. S2-9. Temperature-dependent FL decay profiles and FL lifetimes of BODIPY-C$_{12}$ in 5CB (λ_{ex} = 470 nm and λ_F = 520 nm) for three measurements.
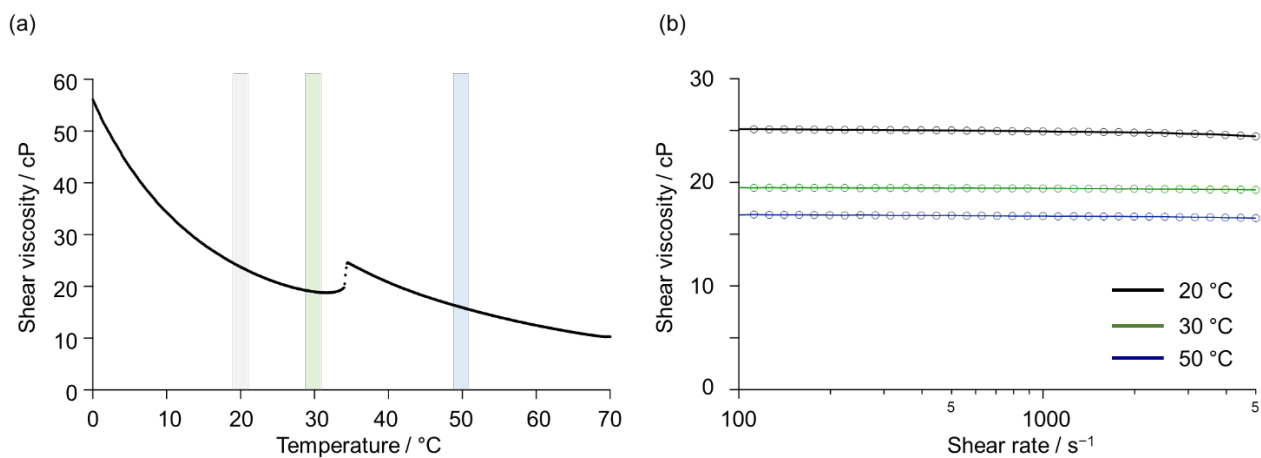
Fig. S2-10. (a) Shear viscosity of 5CB measured by a rheometer (Shear rate: 500 s^{-1}, cooling rate: 6 °C min^{-1}). (b) Shear rate dependence of the shear viscosity of 5CB at each temperature (Shear rate: 100 to 5000 s^{-1}).
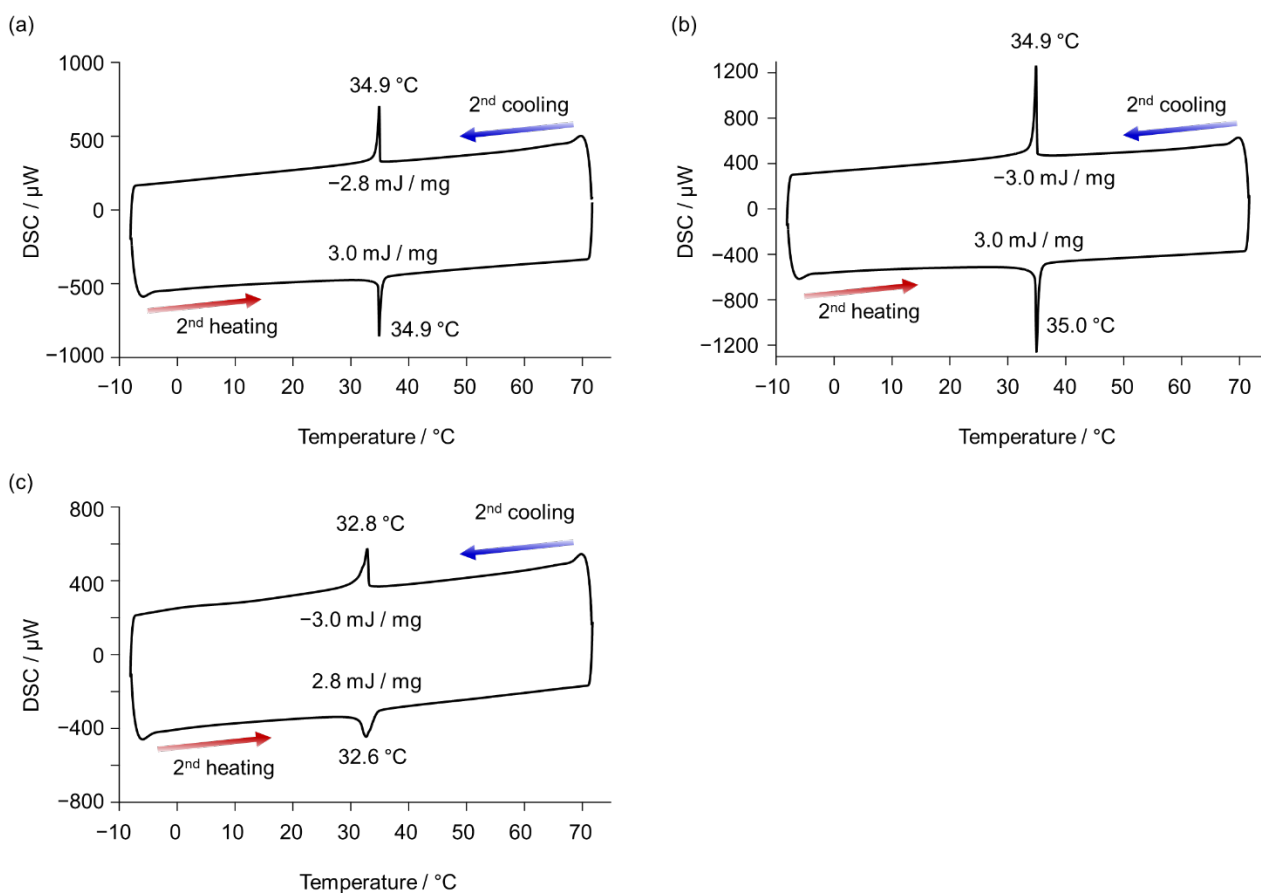

Fig. S2-11. DSC analysis of (a) pure 5CB, (b) 5CB doped with **FLAP0** (0.01 wt%), and (c) 5CB doped with **FLAP0** (1 wt%).

Differential scanning calorimetry (DSC) measurements were conducted under N_2 atmosphere at a flow speed of 30 mL min^{-1}. Heating and cooling processes were shown in Fig. S2-12. Each sample was placed in an aluminum pan and covered with an aluminum cover, which was pressed with a pressing tool. A vacant pan and a cover, which was also pressed, was used as a reference sample.
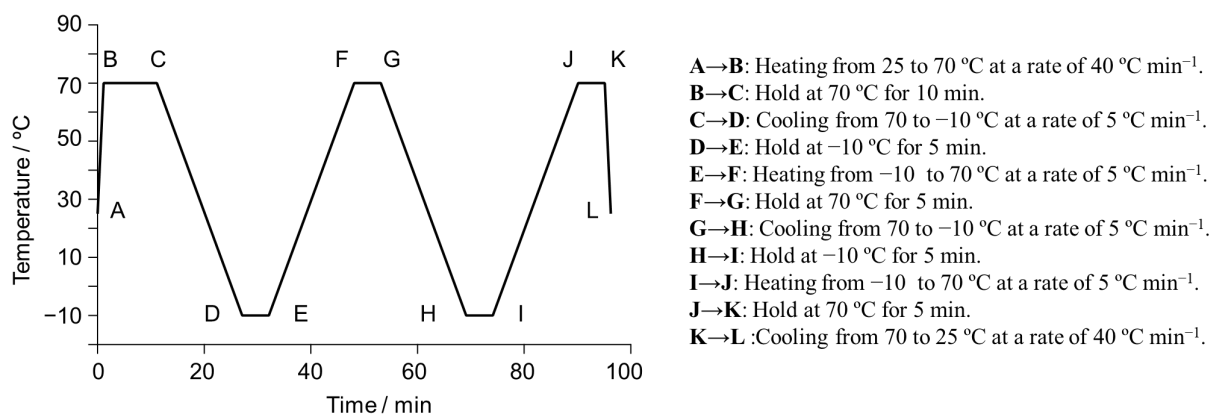

A→B: Heating from 25 to 70 ºC at a rate of 40 ºC min^{-1}.
B→C: Hold at 70 ºC for 10 min.
C→D: Cooling from 70 to −10 ºC at a rate of 5 ºC min^{-1}.
D→E: Hold at −10 ºC for 5 min.
E→F: Heating from −10 to 70 ºC at a rate of 5 ºC min^{-1}.
F→G: Hold at 70 ºC for 5 min.
G→H: Cooling from 70 to −10 ºC at a rate of 5 ºC min^{-1}.
H→I: Hold at −10 ºC for 5 min.
I→J: Heating from −10 to 70 ºC at a rate of 5 ºC min^{-1}.
J→K: Hold at 70 ºC for 5 min.
K→L :Cooling from 70 to 25 ºC at a rate of 40 ºC min^{-1}.

Fig. S2-12. Heating and cooling processes of the DSC measurements.

3. Microscopic measurements
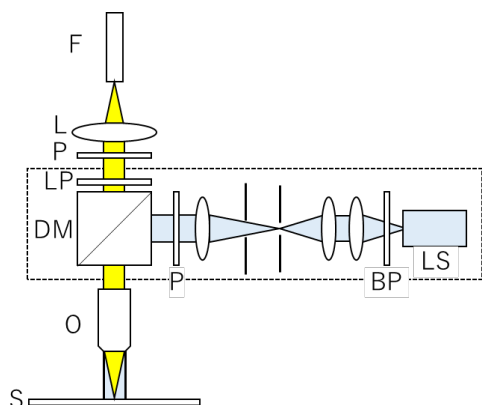
F:Fiber	BP: Band-pass filter
L: Lens	LS: Light-source（LED）
P: Polarizer	O: Objective
LP: Long-pass filter	S: Sample
DM: Dichroic mirror	

- Light Source: Thorlabs M385L2
- Bandpass filter：Nikon Bandpass 330-380
- Dichroic mirror：Semrock Di-405-25x36
- Longpass filter：Edmund OD4.0 Longpass450 nm
- UV Power: 80 μW, spot size: ~340μm（23 mW/cm²）

Fig. S3-1. Experimental setup and conditions of microscopic measurements. The polarizer in the detection path was inserted or removed as necessary. Measurements were made with typical illumination intensities of ~ 80 μW over an illumination spot of ~340 μm (corresponding to ~20 mW/cm²) and no photodegradation was observed during the measurements. For the analysis of the FL intensities at specified wavelengths, the intensities were extracted after applying binomial smoothing of 5 passes on the acquired spectra (performed using Igor Pro Software).
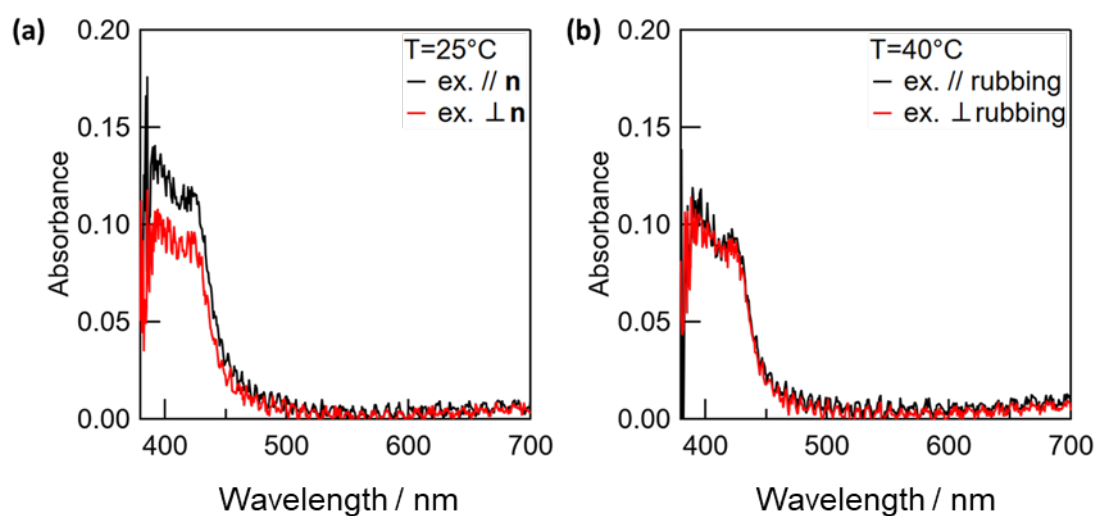

Fig. S3-2. (a) Polarized absorbance spectra of **FLAP0** doped at a concentration of 1 wt% in 5CB, measured along (pol.//**n**) and perpendicular (pol.⊥**n**) to the director of 5CB in the nematic phase (25 °C). (b) Polarized absorbance spectra measured in the isotropic phase (40 °C), where the polarizations are written with reference to the rubbing axis on the substrate.

Note: We found that **FLAP0** doped in 5CB has a small anisotropy in the longer wavelength region of the absorption spectrum ($\lambda > 400$ nm), in which 5CB has no absorption, indicating that the ground-state direction of **FLAP0** is not completely isotropic.

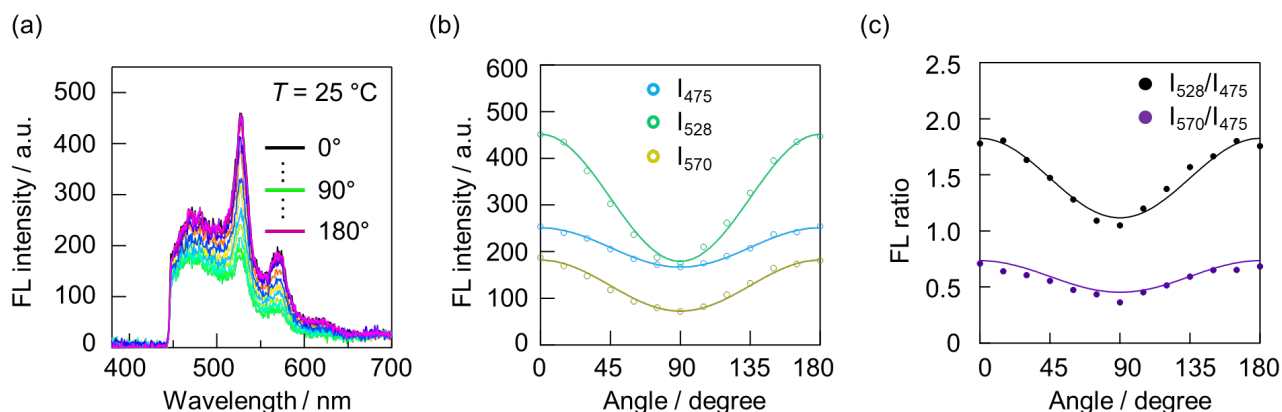**Fig. S3-3.** (a) Polarization-resolved FL spectra (non-polarized excitation, λ_{ex} = 380 nm) of **FLAP0** doped in 5CB (0.5 wt%) in the nematic phase (25 °C), where the polarization angle is measured from the director axis. (b) Dependence of the FL peak intensities on the polarizer angle. (c) Polarization dependence of the FL intensity ratios attributed to the planarized (528, 570 nm) and V-shaped (475 nm) **FLAP0** species in the S_1 excited state.
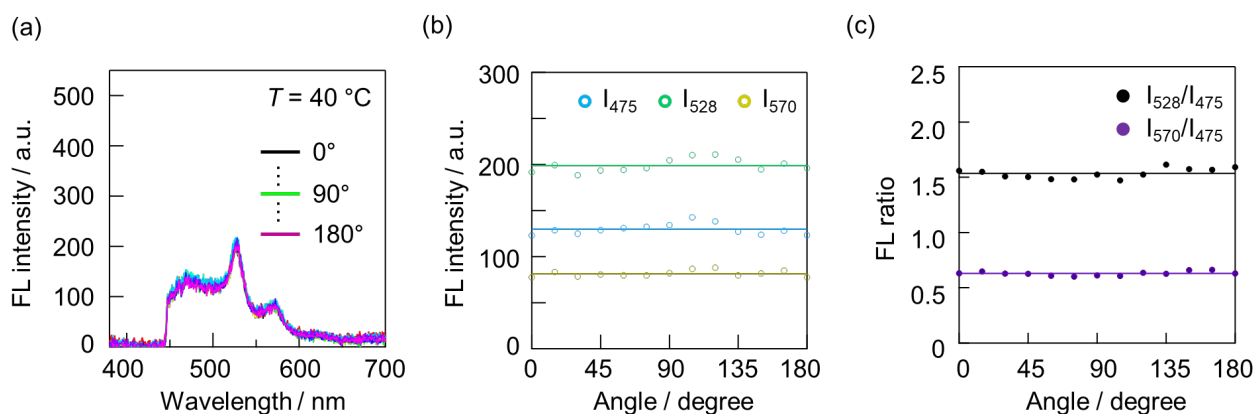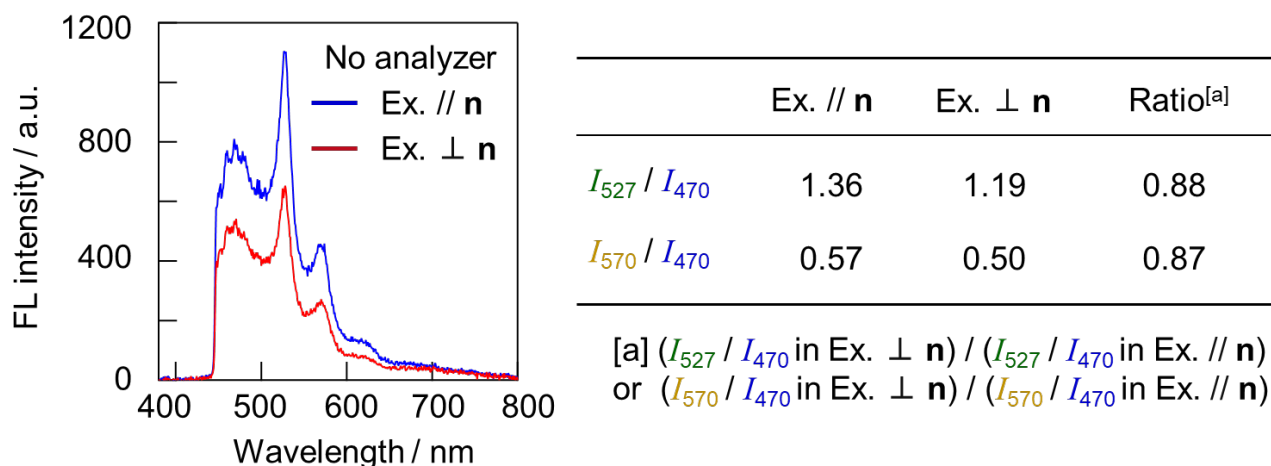

Fig. S3-4. (a) Polarization-resolved FL spectra (non-polarized excitation, λ_{ex} = 380 nm) of **FLAP0** doped in 5CB (0.5 wt%) in the isotropic phase (40 °C). The polarization angle is measured from the rubbing axis on the cell substrates. (b) Dependence of the FL peak intensities on the polarization angle. (c) Polarization dependence of the FL intensity ratios attributed to the planarized (528, 570 nm) and V-shaped (475 nm) **FLAP0** species in the S_1 excited state.

	Ex. // **n**	Ex. ⊥ **n**	Ratio[a]
I_{527} / I_{470}	1.36	1.19	0.88
I_{570} / I_{470}	0.57	0.50	0.87

[a] $(I_{527} / I_{470}$ in Ex. ⊥ **n**) / $(I_{527} / I_{470}$ in Ex. // **n**) or $(I_{570} / I_{470}$ in Ex. ⊥ **n**) / $(I_{570} / I_{470}$ in Ex. // **n**)

Fig. S3-5. FL spectra and FL ratios of **FLAP0** in 5CB (0.5 wt%) at 25 °C excited with a polarized light (λ_{ex} = 380 nm) but detected with the analyzer removed. Ex.//**n** and Ex.⊥**n** indicate excitation polarizations parallel and perpendicular to the 5CB director, respectively.

Note: When **FLAP0** was excited with a polarized light and the FL was detected without an analyzer, the FL ratio showed a significant dependence on the polarization angle of the excitation light. This means that the degree of the suppression of the planarization dynamics is dependent on the direction of the V-shaped **FLAP0** in the ground state relative to the director of 5CB.
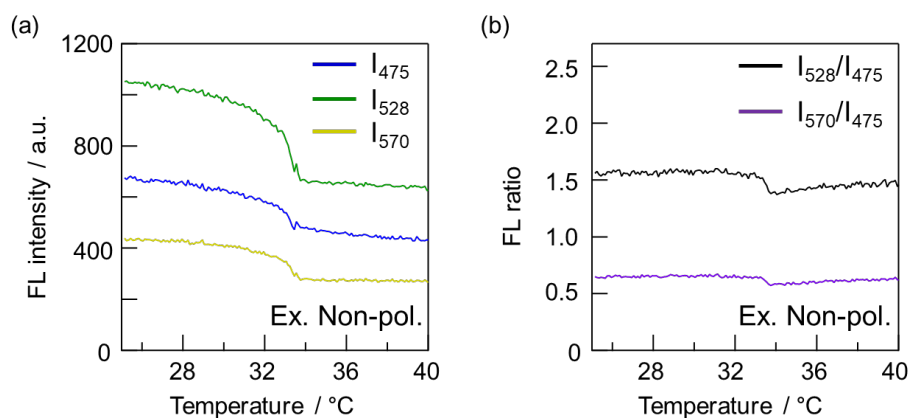
Fig. S3-6. Temperature dependence of (a) the FL intensities and (b) the FL ratios of **FLAP0** doped in 5CB (0.5 wt%) excited with a non-polarized light (λ_{ex} = 380 nm) and detected without passing a polarizer. A kink is observed in the FL ratio at approx. 34 °C, demonstrating ratiometric detection of the phase transition by **FLAP0**.

4. Density functional theory (DFT) calculations

DFT calculations of the isolated molecules were performed using the Gaussian 16 program.[S7] Kohn–Sham orbitals were displayed by the Avogadro program.[S8] A model structure (**FLAP0′**) has hydrogen atoms in place of the 2,6-diisopropylphenyl groups of the corresponding molecule (**Fig. S4-1**).
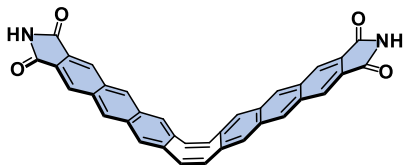

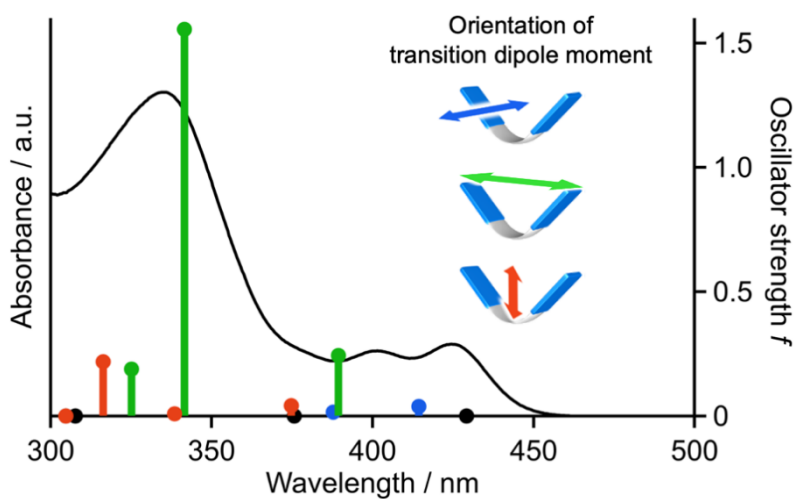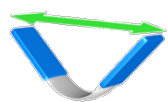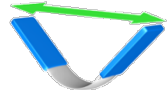**Fig. S4-1.** The model compound **FLAP0′** for the DFT calculations.

Fig. S4-2. Oscillator strengths of $S_0 \rightarrow S_n$ transitions of **FLAP0′** (optimized geometry in S_0) calculated at the TD-PBE0/6-31+G(d) level (bars) and observed UV-visible absorption spectrum (line) of **FLAP0** in PhCN.

Table S4-1. Excitation energies and oscillator strengths for **FLAP0′** (optimized geometry in S_0) calculated at the TD-PBE0 /6-31+G(d) level.

| Transition	Excitation energy	Configurations	f	Orientation of transition dipole moment
$S_0 \rightarrow S_1$	2.89 eV (429 nm)	HOMO $\rightarrow$ LUMO (96%)	0	—
$S_0 \rightarrow S_2$	2.99 eV (414 nm)	HOMO $\rightarrow$ LUMO+1 (92%) HOMO−1 $\rightarrow$ LUMO (7%)	0.0382	
$S_0 \rightarrow S_3$	3.18 eV (389 nm)	HOMO $\rightarrow$ LUMO+2 (70%) HOMO−2 $\rightarrow$ LUMO (16%) HOMO−1 $\rightarrow$ LUMO+3 (8%)	0.2438	
$S_0 \rightarrow S_4$	3.20 eV (388 nm)	HOMO−1 $\rightarrow$ LUMO (92%) HOMO $\rightarrow$ LUMO+1 (7%)	0.0153	
$S_0 \rightarrow S_5$	3.30 eV (376 nm)	HOMO−1 $\rightarrow$ LUMO+1 (96%)	0	—
$S_0 \rightarrow S_6$	3.31 eV (375 nm)	HOMO $\rightarrow$ LUMO+3 (37%) HOMO−1 $\rightarrow$ LUMO+2 (29%) HOMO−2 $\rightarrow$ LUMO+1 (24%)	0.0421	
$S_0 \rightarrow S_7$	3.63 eV (342 nm)	HOMO−2 $\rightarrow$ LUMO (75%) HOMO $\rightarrow$ LUMO+2 (22%)	1.5553	
$S_0 \rightarrow S_8$	3.66 eV (339 nm)	HOMO $\rightarrow$ LUMO+3 (53%) HOMO−1 $\rightarrow$ LUMO+2 (41%)	0.0089	
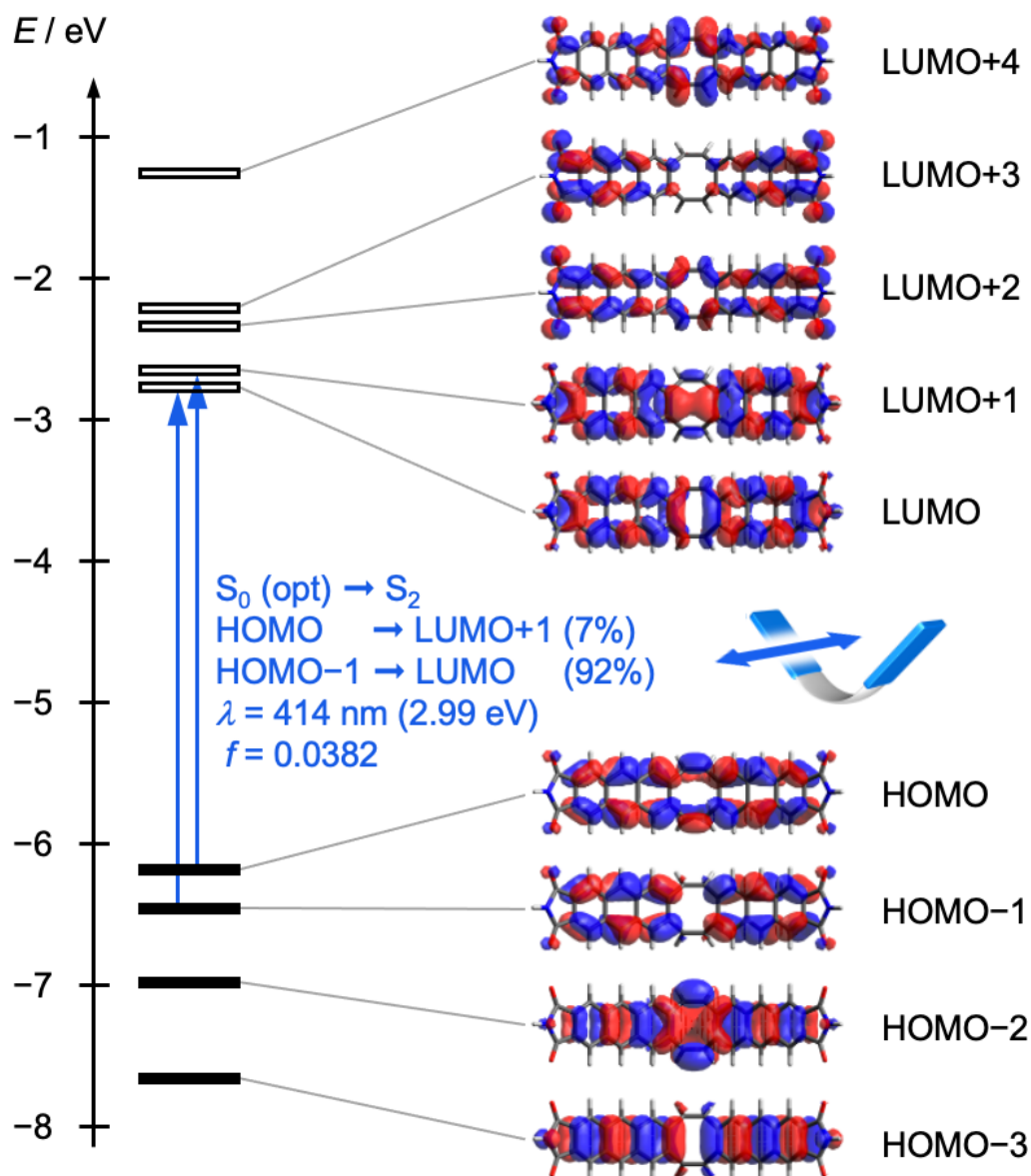
Fig. S4-3. Kohn–Sham molecular orbitals of **FLAP0′** in the S_0 optimized geometry (C_{2v} symmetry, COT bending angle $\theta = 41.1°$) and the transition character of the absorption in the longest wavelength region, calculated at the (TD-)PBE0/6-31+G(d) level. See the reference [S2] for the definition of the COT bending angle.
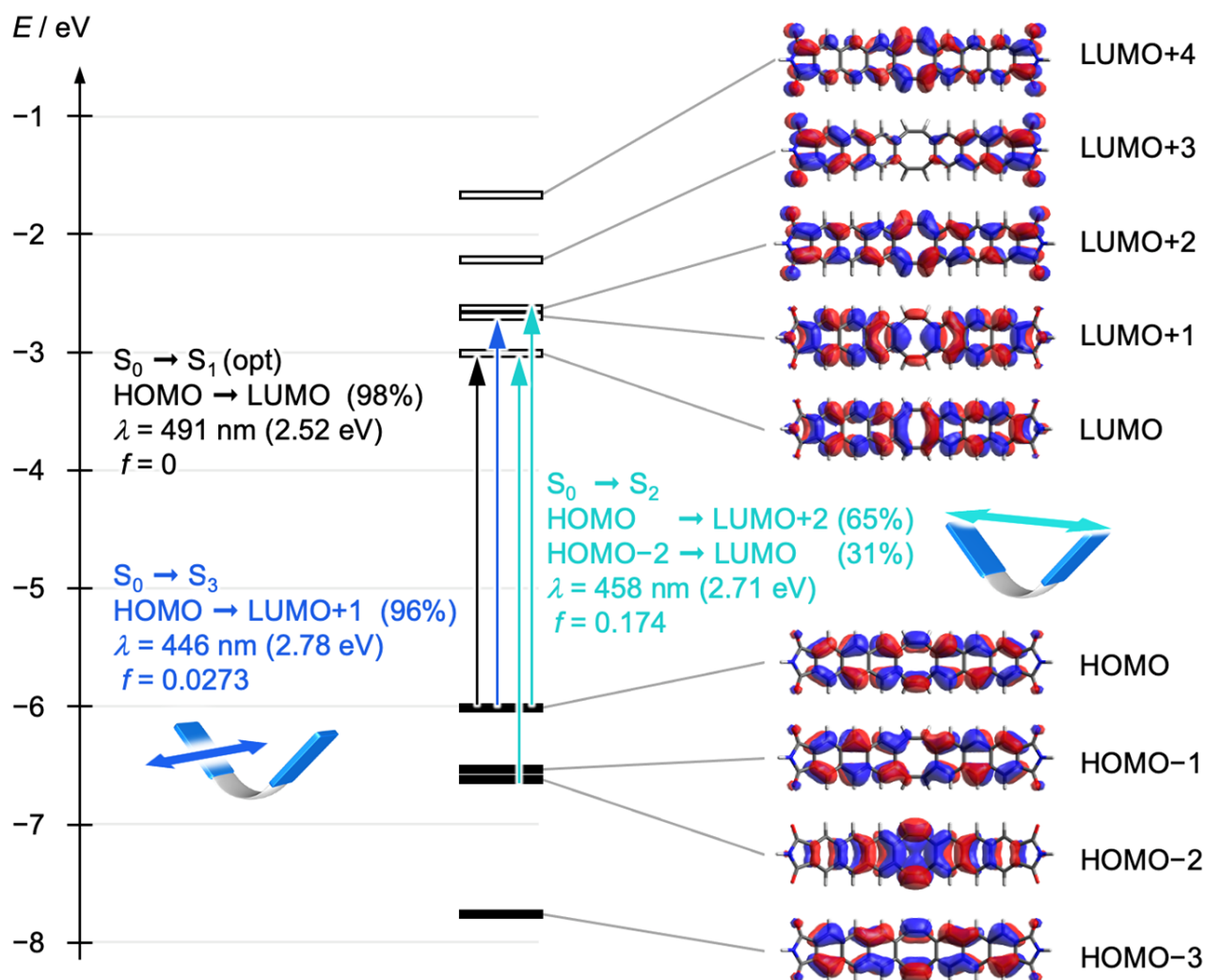
Fig. S4-4. Kohn–Sham molecular orbitals of **FLAP0′** with the shallow V-shaped structure (C_{2v} symmetry) at the S_1 local minimum (COT bending angle $\theta = 28.2°$) and the transition characters, calculated at the TD-PBE0/6-31+G(d) level. See the reference [S2] for the definition of the COT bending angle.
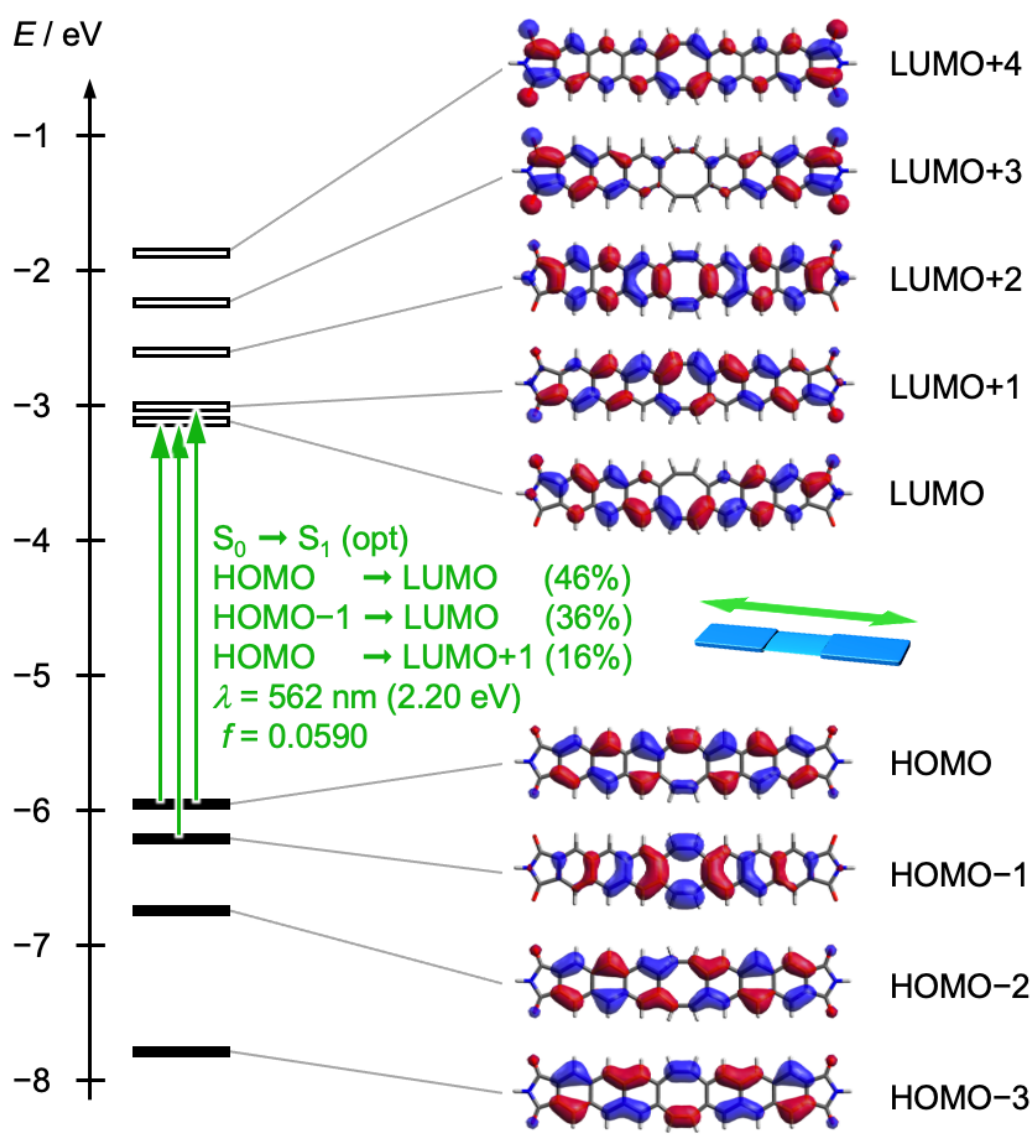
Fig. S4-5. Kohn–Sham molecular orbitals of **FLAP0′** with the planar structure (C_{2v} symmetry) at the S_1 global minimum (COT bending angle $\theta = 0°$) and the transition character of the fluorescence, calculated at the TD-PBE0/6-31+G(d) level. See the reference [S2] for the definition of the COT bending angle.

5. Supplementary references

S1. R. Kotani, H. Sotome, H. Okajima, S. Yokoyama, Y. Nakaike, A. Kashiwagi, C. Mori, Y. Nakada, S. Yamaguchi, A. Osuka, A. Sakamoto, H. Miyasaka and S. Saito, *J. Mater. Chem. C* **2017**, *5*, 5248.

S2. R. Kimura, H. Kuramochi, P. Liu, T. Yamakado, A. Osuka, T. Tahara and S. Saito, *Angew. Chem. Int. Ed.* **2020**, *59*, 16430.

S3. M. K. Kuimova, G. Yahioglu, J. A. Levitt and K. Suhling, *J. Am. Chem. Soc.* **2008**, *130*, 6672.

S4. W. Nakanishi, S. Saito, N. Sakamoto, A. Kashiwagi, S. Yamaguchi, H. Sakai and K. Ariga, *Chem. Asian J.* **2019**, *14*, 2869.

S5. R. Kimura, H. Kitakado, A. Osuka and S. Saito, *Bull. Chem. Soc. Jpn.* **2020**, *93*, 1102.

S6. P. Loison, Neveen, A. Hosny, P. Gervais, D. Champion, M. K. Kuimova, and J.-M. Perrier-Cornet, *Biochimica et Biophysica Acta* **2013**, *1828*, 2436.

S7. Gaussian 16, Revision A.03, M. J. Frisch, G. W. Trucks, H. B. Schlegel, G. E. Scuseria, M. A. Robb, J. R. Cheeseman, G. Scalmani, V. Barone, G. A. Petersson, H. Nakatsuji, X. Li, M. Caricato, A. V. Marenich, J. Bloino, B. G. Janesko, R. Gomperts, B. Mennucci, H. P. Hratchian, J. V. Ortiz, A. F. Izmaylov, J. L. Sonnenberg, D. Williams-Young, F. Ding, F. Lipparini, F. Egidi, J. Goings, B. Peng, A. Petrone, T. Henderson, D. Ranasinghe, V. G. Zakrzewski, J. Gao, N. Rega, G. Zheng, W. Liang, M. Hada, M. Ehara, K. Toyota, R. Fukuda, J. Hasegawa, M. Ishida, T. Nakajima, Y. Honda, O. Kitao, H. Nakai, T. Vreven, K. Throssell, J. A. Montgomery, Jr., J. E. Peralta, F. Ogliaro, M. J. Bearpark, J. J. Heyd, E. N. Brothers, K. N. Kudin, V. N. Staroverov, T. A. Keith, R. Kobayashi, J. Normand, K. Raghavachari, A. P. Rendell, J. C. Burant, S. S. Iyengar, J. Tomasi, M. Cossi, J. M. Millam, M. Klene, C. Adamo, R. Cammi, J. W. Ochterski, R. L. Martin, K. Morokuma, O. Farkas, J. B. Foresman, and D. J. Fox, Gaussian, Inc., Wallingford CT, **2016**.

S8. M. D. Hanwell, D. E. Curtis, D. C. Lonie, T. Vandermeersch, E. Zurek and G. R. Hutchison, *J. Cheminfomatics* **2012**, *4*, 17.